Functional and structural analysis of a catabolite control protein C that responds to citrate

Wei Liu
Dalian Minzu University
Jinli Chen
Dalian University of Technology
Liming Jin
Dalian Minzu University
Zi-Yong Liu
Qingdao Institute of Bioenergy and Bioprocess Technology
Ming Lu
Qingdao Institute of Bioenergy and Bioprocess Technology
Ge Jiang
Dalian University
Qing Yang
Dalian University of Technology
Chunshan Quan
Dalian Minzu University
Ki Hyun Nam
Pohang University of Science and Technology
Yongbin Xu (yongbinxu@dlnu.edu.cn)
Dalian Minzu University

Research Article

Keywords: Catabolite control protein C (CcpC), Bacillus amyloliquefaciens (BaCcpC-FL)

Posted Date: March 13th, 2021

DOI: https://doi.org/10.21203/rs.3.rs-287355/v1

Abstract

Catabolite control protein C (CcpC) belongs to the LysR-type transcriptional regulator (LTTR) family that regulates the transcription of genes encoding the tricarboxylic acid branch enzymes of the TCA cycle by responding to a pathway-specific metabolite, citrate. The biological function of CcpC has been characterized several times, but the structural basis for the molecular function of CcpC remains elusive. Here, we report characterization of a full-length CcpC from *Bacillus amyloliquefaciens* (BaCcpC-FL) and a crystal structure of the C-terminal inducer-binding domain (IBD) complexed with citrate. BaCcpC required both dyad symmetric regions I and II to recognize the *citB* promoter, and the presence of citrate reduced *citB* promoter binding. The crystal structure of CcpC-IBD shows two subdomains, IBD-I and IBD-II, and a citrate molecule buried between them. Ile100, two arginines (Arg147 and Arg260), and three serines (Ser129, Ser189, and Ser191) have strong hydrogen-bond interactions with citrate molecules. A structural comparison of BaCcpC-IBD with its homologues shows that they share the same tail-to-tail dimer alignment, but the dimeric interface and the rotation between these molecules exhibit significant differences. In addition, citrate can convert large BaCcpC-FL oligomers to monomers in solution. Taken together, our results provide a framework for understanding the mechanism underlying the functional divergence of the CcpC protein.

Introduction

The tricarboxylic acid (TCA) cycle, also known as the Krebs cycle or the citric acid cycle (CAC), is a central metabolic pathway in the cell [1]. The TCA cycle provides organisms with reducing potential, energy, and three of the 13 biosynthetic intermediates [2]. In *Bacillus*, TCA activity is controlled by several important regulatory proteins, including global regulators CcpA and CodY and the specific regulator CcpC, which are coordinated by fructose-1,6-bisphosphate (FBP) and glucose-6-phosphate, guanosine-5'-triphosphate (GTP) and branched-chain amino acids (BCAAs), and citrate, respectively [3]. CcpA and CodY are metabolite-responsive global regulators of carbon metabolism pathways [4]. These global regulators coordinate the expression of numerous metabolic, biosynthetic and virulence genes that respond to three metabolites [5]. CcpA is a member of the LacI/GalR family of transcriptional repressors, which exert both direct (through citrate synthase, *citZ*, and *ccpC*) and indirect effects on TCA branch enzyme expression [6]. CodY is also a repressor of the *citB* gene belonging to a unique family of regulators in *B. subtilis* and other homologues of gram-positive bacteria [7]. Recent studies showed that CcpC and CcpE exclusively regulate the TCA branch enzymes of the TCA cycle (*citB*, aconitase; *citC*, isocitrate dehydrogenase; and *citZ*, citrate synthase) by responding to a pathway-specific metabolite for both *Bacillus subtilis* and *Staphylococcus aureus*, respectively [8 9].

CcpC widely exists in prokaryotes and is classified in the LysR-type transcriptional regulator (LTTR) family [10]. Typical LTTR family proteins comprise approximately 330 amino acids that form structures highly similar to those of N-terminal DNA-binding domains (DBDs), which are directly involved in DNA interactions, and poorly conserved C-terminal inducer-binding domains (IBDs) and are known to adopt

different oligomeric states [10]. The DBD is highly conserved and directly involved in DNA interactions, similar to the helix-loop-helix, zinc finger, and β–sheet-anti-parallel domains [11 12 13]. The role of IBD transcription factors in the regulation of bacterial virulence has been investigated in many pathogenic organisms. The coinducer citrate is important for the function of CcpC and appears to function as a key catabolite for coordinating the *B. subtilis* metabolic state by binding to and activating CcpC [9]. Thus, the CcpC complex with citrate is a signal that morphs CcpC into a conformation that is competent for binding DNA and gene transcription. Several biological functional properties of CcpC are well characterized; however, the structure-based molecular function has been elusive [9].

In this study, we characterized the full-length *Bacillus amyloliquefaciens* CcpC and determined the crystal structure of the C-terminal IBD of *B. amyloliquefaciens* CcpC (BaCcpC-IBD) at 2.3 Å resolution. The *citB* binding properties and the oligomeric state of BaCcpC were analysed. The crystal structure of BaCcpC-IBD was compared with structures of the LTTR family members. Taken together, our findings provide insight into the citrate-responsive mechanism of CcpC.

Results And Discussion

Biochemical study of BaCcpC

In *B. subtilis*, CcpC (BsCcpC) negatively regulates *citB* gene expression, which is responsible for the interconversion of citrate and isocitrate [9]. The BsCcpC binding region forms two dyad symmetry elements centred at positions − 66 and − 27 (Fig. 1A) [9]. These BsCcpC bind to the DNA-binding boxes “ATAA”, “TTAT”, and “TATT” in the *citB* promoter region [9]. In the *B. amyloliquefaciens* genome, the potential promoter region of *citB* (named *citB*-P) was found from position − 73 to -20, and it shows high similarity with the same DNA-binding boxes “ATAA”, “TTAT”, and “TATT” (Fig. 1A). The DNA sequence of the BsCcpC binding box was identical to that of the BaCcpC binding box in *citB* promoter region I (named *citB*-PI, -73 to -54), but the nonbinding sequences did not match, whereas the DNA sequences of *citB* promoter region II (named *citB*-PII, -40 to -20) matched a consensus sequence (Fig. 1A). Meanwhile, the spacer sequence between *citB* protomer regions I and II was identical to those of *B. subtilis* and *B. amyloliquefaciens*, as was the DNA length.

To verify whether CcpC regulates the predicted *citB* promoter region in *B. amyloliquefaciens*, we performed an electrophoretic mobility shift assay (EMSA) using a 56 bp *citB* promoter DNA fragment (from nucleotides − 73 to -20 relative to the start codon of *citB*) as a probe (Fig. 1A). A complete shift of the free probe was observed as the concentration of BaCcpC increased (Fig. 1B). This result indicates that BaCcpC has a high binding affinity for *citB* promoter DNA of *B. amyloliquefaciens*. Next, the binding of BaCcpC to each of the *citB* promoter regions (I and II) for each CcpC was assessed. BaCcpC did not bind to either promoter region (Fig. 1C-D). These results indicate that both dyad symmetry promoter regions are required for BaCcpC to bind to the promoter of *citB*. To determine whether citrate affects the binding of CcpC to the *citB* promoter, an EMSA of CcpC for *citB* was performed with citrate. The results showed that the presence of citrate slightly suppressed the binding of CcpC to *citB*-P (Fig. 1E).

Oligomerization of BaCcpC

LTTRs are usually functionally active as tetramers and dependent upon a coinducer [14]. To verify the oligomeric state of BaCcpC (MW ~ 30 kDa) in solution, we performed size exclusion chromatography. The chromatogram showed multiple peaks (Fig. 2A). The calculated molecular weights of BaCcpC for the first and second peaks were > 500 kDa and 30 kDa, respectively. This result indicated that BaCcpC exists as a large oligomer (or aggregated form) or a monomer in solution. Meanwhile, in equilibrium buffer with 10 mM citrate, the abundance of the large oligomer, i.e., the first peak intensity, was reduced, whereas the monomer population, i.e., the second peak, was increased (Fig. 2A). These results indicated that citrate induced the oligomers of BaCcpC proteins to form monomers but not completely. In the crystal structure of BaCcpC-IBD, citrate molecules interact directly with two serine residues (Ser189 and Ser191) by forming hydrogen bonds (see below). To understand whether these two serine residues influence the oligomeric state of BaCcpC mutants (Ser189Ala and Ser191Ala, named BaCcpC-S189A and BaCcpC-S191A), we performed size exclusion chromatography. Interestingly, when we assessed the oligomeric states of BaCcpC-S189A and BaCcpC-S191A, only one peak appeared (MW ~ 30 kDa) (Fig. 2B).

Overall structure of the IBD of BaCcpC

To better understand the molecular function of BaCcpC, we performed a crystallographic study on full-length BaCcpC; however, it was not successful. Furthermore, crystallographic studies for the DBD and IBD of BaCcpC were separately performed. Finally, we obtained crystals for the IBD of BaCcpC and determined the crystal structure of BaCcpC-IBD in complex with citrate at 2.3 Å resolution using single-wavelength anomalous diffraction (SAD) phasing. The BaCcpC-IBD crystal belonged to space group C2 and had unit-cell parameters of a = 140.96, b = 90.90, c = 105.53 Å and β = 106.18°. The R_{work} and R_{free} of the final model were 20.7% and 26.6%, respectively. The BaCcpC-IBD molecule is composed of two distinct regulatory domains: IBD-I (His90-Arg155 and Gly266-Gln289) and IBD-II (Asp168-Gly259) (Fig. 3A). IBD-I has three β-sheets, which are surrounded by three α-helices and 3_{10} helices (Fig. 3B). IBD-II has four β-sheets, which are surrounded by two α-helices and two 3_{10} helices (Fig. 3B). Both IBD-I and IBD-II subdomains adopt the typical α/β fold, which is connected by two crossover regions that form a hinge at central regions of two antiparallel β-strands (β4 and β9) (Fig. 3A). Five BaCcpC-IBD molecules are in the asymmetric unit, and each molecule has an r.m.s.d. of 0.201–0.275 Å for the 144–180 Cα atoms, which emphasizes the similarity of their conformations. BaCcpC-IBD forms dimers with a head-to-tail arrangement in the asymmetric unit of its crystal structure, and both molecules have essentially the same overall structure (Fig. 3C). Superposition of two dimeric molecules in the asymmetric unit gives an r.m.s.d. of 0.327 Å for 321 Cα. The dimeric interface is stabilized by the main chain interactions Val122-Thr212* (2.82 Å, * denoting the partner molecule), Val122-Leu214* (2.92 Å), Leu124-Asp216* (2.80 Å), and Thr126-Asp216* (3.33 Å) between the β2 strand and β6 strand (Fig. 3D).

The citrate binding site of BaCcpC-IBD

To observe the citrate-bound state of BaCcpC-IBD, we added sodium citrate to the purification buffer during all protein purification steps. The electron density corresponding to citrate molecules is found at the positively charged interface between IBD-I and IBD-II of BaCcpC-IBD (Fig. 4A). In the electron density

map, the positions of each carboxyl and hydroxyl group of citrate are clearly distinguished (Fig. 4A). Citrate is a small organic acid that includes three carboxyl groups, one hydroxyl group, and one prochiral centre. To distinguish between the terminal carboxyl groups, they were named *pro-R* and *pro-S*. The *pro-R* carboxyl group accepts a strong hydrogen bond from the backbone nitrogen atom of Ile100 (average distance for five molecules in the asymmetric unit: 3.12 Å). In addition, the pro-S carboxyl group also has hydrogen bonds from the side-chain NE atoms of Arg147 (2.93 Å) and Arg260 (2.80 Å). The central carboxyl group of citrate accepts hydrogen bonds from the backbone nitrogen atom of Ser129 (2.70 Å), the side-chain hydroxyl group, and Ser189 (2.59 Å) and Ser191 (2.89 Å). The hydroxyl group of citrate interacts with the side-chain hydroxyl group of Ser129 (2.76 Å). The atoms of these residues that contact the citrate molecule are ~ 3.0 Å away from the latter's oxygen atoms, demonstrating that the citrate was coordinated by extensive strong hydrogen-bonding interactions (Fig. 4A).

Inducers are important for the function of LTTRs and often participate in the feedback loop of a specific metabolic/synthesis pathway [15]. However, citrate molecules are inducers for BaCcpC, BsCcpC, and SaCcpE [8 9]. Sequence alignment shows that the Arg147 and Arg260 residues of BaCcpC are highly conserved in both BsCcpC and SaCcpE, whereas Ile100, Ser129, Ser189, and Ser191 of BaCcpC are not conserved in SaCcpE, being conserved in only BsCcpC (Fig. 4B). Moreover, the citrate-binding Arg147 and Arg260 residues of BaCcpC-IBD analogous to the citrate-binding Arg145 and Arg256 residues of CcpE, which are required for CcpE to evoke an appropriate response in the presence of citrate [16 17] (Fig. 4C). Therefore, we consider these two arginine residues to also play important roles in the citrate binding and functional assembly of BaCcpC.

Comparison of BaCcpC-IBD with other IBDs from the LTTR family

To better understand the structural properties of BaCcpC-IBD, its homologues were sought using the Dali server. The IBD of CcpE from *S. aureus* (named SaCcpE-IBD, Z-score: 22.0, sequence identity: 28%, Protein Data Bank (PDB) code: 4QBA), C-terminal domain of a putative transcriptional regulator from *Klebsiella pneumoniae* (KpYneJ-CTD, 20.6, 19%, 5TPI) and ligand-binding domain of OccR from *Agrobacterium tumefaciens* (AtOccR-LBD, 19.3, 17%, 5VVH) showed structural similarity to BaCcpC. These proteins belong to the LTTR family. BaCcpC is involved in citrate metabolism, similar to SaCcpE, while AtOccR and KpYneJ are involved in octopine catabolism and biosynthesis of cysteine, respectively [8 18 19]. Although BaCcpC-IBD shared low amino acid sequence identities (less than 30%) with SaCcpE-IBD, KpYneJ-CTD, and AtOccR-LBD, they are commonly composed of two subdomains, similar to IBD-I and IBD-II of BaCcpC-IBD (Fig. 5A). Superposition of BaCcpC-IBD with SaCcpE-IBD-apo, SaCcpE-IBD-citrate, KpYneJ-CTD, and AtOccR-LBD shows structural similarity with RMSDs of 1.818 Å, 1.181 Å, 2.240 Å and 1.941 Å, respectively.

SaCcpE-IBD, KpYneJ-CTD, and AtOccR-LBD also show dimers with the same tail-to-tail alignments as BaCcpC-IBD, but the dimeric interfaces and the rotations between these molecules exhibit significant differences. The dimeric interface of SaCcpE-IBD is formed by hydrogen bonds as well as some salt bridges between α1 and α5*, α1 and loop*, and loop and loop* (an asterisk indicates the partner molecule) (Fig. 5B). The dimer interface of KpYneJ-CTD consists of two α-helices that interact with one β-

sheet, namely, α1-α5*, β2-α5*, α5-β2* and α5-α1*, which differ from the dimer interface of AtOccR-LBD in α1-α5*, loop-loop* and β2-β7* (Fig. 5B and Supplementary Fig. 1). These findings indicated that IBD dimers are relatively stable, even after poor conservation in IBDs. Meanwhile, the rotation angles of dimers are distinct. In addition, CcpC-IBD is functionally distinct from CcpE-IBD but also recognizes citrate molecules. The monomers of citrate-bound BaCcpC-IBD and SaCcpE-IBD dimers are rotated at angles of approximately 33° and 35°, respectively (Fig. 5C). As a result, the rotation angle of the dimer interface of citrate-bound BaCcpC-IBD is very similar to that of citrate-bound SaCcpE-IBD. On the other hand, in the citrate-free state of SaCcpE-IBD, the angle of the dimer interface is approximately 80°, indicating that there is a change in dimer formation depending on citrate binding. Accordingly, the dimeric interface of in BaCcpC-IBD differs when citrate is absent or bound.

Conclusion

BaCcpC required both dyad symmetry regions I and II for recognizing the *citB* promoter, and the presence of citrate reduced *citB* binding. Citrate binds the interface between IBD-I and IBD-II of the IBD of BaCcpC. The IBD of BaCcpC shares low sequence similarity with other IBDs of the LTTR family but is similar in terms of the overall structure and dimer formation. Our results provide the framework for a functional analysis of CcpC as well as the diversity and similarity of IBDs of the LTTR family.

Methods

Construction, expression, and purification

The full-length (residues 1-293; named BaCcpC-FL) and C-terminal region of the IBD (residues 88–293; named BaCcpC-IBD) of CcpC were obtained from genomic DNA of *B. amyloliquefaciens* by PCR. The gene was cloned into the *Nco*I and *Xho*I sites of the pPROEX-HTA vector (Invitrogen, USA), which contains a hexahistidine tag (MSYYHHHHHH), a spacer region (DYDIPTT) and a tobacco etch virus (TEV) protease cleavage site (ENLYFQ) at the N-terminus. The construct was transformed into *E. coli* BL21 (DE3) competent cells to obtain the target proteins. Protein expression and purification procedures were the same for BaCcpC-FL and BaCcpC-IBD. Cells were grown in 2 L of Luria-Bertani (LB) medium containing 0.5 μg ml^{-1} ampicillin at 310 K. When the OD_{600} of the culture reached 0.8, 0.5 mM isopropyl-β-d-thiogalactoside (IPTG) was added, and the culture was incubated at 303 K for 8 h. The bacterial cells were centrifuged for harvesting and resuspended in lysis buffer containing 20 mM Tris (pH 8.0), 10 mM sodium citrate, 150 mM NaCl, and 2 mM β-mercaptoethanol. Then, the cells were disrupted by sonication, and the lysate was centrifuged at 13000 rpm for 30 min at 277 K. The lipid fractions were mixed with a nickel-nitrilotriacetic acid (Ni-NTA) affinity resin (GE Healthcare) that had been preincubated with lysis buffer and stirred for 30 min at 277 K. The resin was washed and eluted with lysis buffer containing 20 mM imidazole and 300 mM imidazole. The fractions containing BaCcpC were pooled, and β-mercaptoethanol was added to 10 mM (final concentration). To remove the hexahistidine tag, the mixture was incubated with a recombinant TEV protease at 298 K overnight. For further purification, the mixture was diluted 4-fold using 20 mM Tris (pH 8.0) buffer and loaded onto a Q anion-exchange column (HiTrap-

Q; GE Healthcare, USA). The fractions containing BaCcpC were purified using a HiLoad Superdex 200 gel filtration column (GE Healthcare, USA) pre-equilibrated with buffer containing 20 mM Tris (pH 8.0), 10 mM sodium citrate, 150 mM NaCl and 2 mM β-mercaptoethanol. To express selenomethionine (Se-Met)-substituted CcpC-IBD protein, the bacterial cells were cultured in 1 L of M9 medium supplemented with an amino acid mixture containing L-(+)-Se-Met at 310 K. When the OD_{600} was between 0.6 and 0.8, the cells were induced with 0.5 mM IPTG for 8 h. The Se-Met-substituted protein was purified under the same conditions as the native protein. To obtain crystal structures of BaCcpC-IBD bound to citrate, we added 10 mM sodium citrate throughout the whole purification process. During purification, the presence of the proteins was detected by sodium dodecyl sulfate-polyacrylamide gel electrophoresis (SDS-PAGE) in a 15% gel with Coomassie blue R-250 for staining.

Electrophoretic mobility shift assay (EMSA) experiments

A chemiluminescent EMSA kit was purchased from Beyotime Biotechnology (Nanjing, China), and a biotin-labelled *B. amyloliquefaciens citB* promoter was synthesized by Generation (Wuhan, China). Supplementary Table S1 provides the list of oligonucleotide sequences used for EMSA analysis. EMSA experiments between BaCcpC and *citB* promoter DNA were performed at room temperature. For EMSA between BaCcpC and the *citB* protomer, various concentrations of purified BaCcpC (2.5–40 μM) protein were incubated with *citB* promoter (800 nM) for 30 min. For EMSA of BaCcpC with regions I and II of the *citB* promoter, purified BaCcpC (40 μM) protein was incubated with each *citB* promoter (800 nM). To determine the effect of citrate on binding between BaCcpC and the *citB* promoter, BaCcpC (40 μM) protein was incubated with *citB* promoter (800 nM) with various citrate concentrations (0–70 μM) for 30 min. After incubation, the reaction mixture was placed in a 6% acrylamide gel on ice using 0.5×Tris/Borate/EDTA (TBE) buffer. The product was analysed by chemiluminescence detection on the Tanon 4600 Chemiluminescent Imaging system (Tanon, China).

Size exclusion chromatography

The oligomer states of BaCcpC-FL and BaCcpC-IBD were analysed using gel filtration chromatography. Five hundred microlitres of the BaCcpC-FL or BaCcpC-IBD protein that had been incubated with 10 mM sodium citrate or not was loaded into a Superdex 200 10/300 GL column (GE Healthcare) at 295 K with a flow rate of 0.5 ml min^{-1}; this column had been was pre-equilibrated with 20 mM Tris buffer (pH 8.0) containing 150 mM NaCl and 2 mM 2-mercaptoethanol.

Crystallization, data collection, structure determination, and refinement

BaCcpC-IBD was concentrated to 20 mg ml^{-1} using a Vivaspin centrifugal concentrator (Cut-off: 10 kDa, Millipore, USA). The initial crystallization was performed using the sitting-drop vapour-diffusion method at 295 K using a Crystal Screen HT high-throughput reagent kit (Hampton Research, USA). Crystals of BaCcpC-IBD were grown in 10% polyethylene glycol 6000, 5% 2-Methyl-2,4-pentanediol (MPD), and 0.1 M HEPES (pH 7.5) using a 1:1 ratio of protein to mother liquor at 287 K. Finally, crystals of BaCcpC-IBD were obtained in sitting drops over 8% (w/v) polyethylene glycol 6000, 6% MPD, and 0.1 M HEPES (pH 7.5) using a 1:1 ratio of protein to mother liquor at 287 K. Immediately after the single crystals were taken

from their drop, they were soaked for 5 s in cryoprotectant solution consisting of the mother liquor solution containing 25% (v/v) glycerol and subsequently flash-cooled in liquid nitrogen.

The dataset was collected at 100 K using an ADSC Q310 CCD detector at Beamline 7A, Pohang Accelerator Laboratory (Pohang, Republic of Korea). The peak wavelength of Se-Met in BaCcpC was determined to be 0.9826 Å by a fluorescence scan. Data were collected using the inverse beam method with an oscillation range of 1° per frame over a 360° rotation, and the exposure time was 5 sec per frame. The crystal of the BaCcpC-IBD protein diffracted to 2.3 Å resolution. Diffraction data were processed, merged, and scaled using the *HKL*-2000 program [20]. Initial phases were obtained using AUTOSOL in the software package PHENIX [21]. Refinement was performed using the Crystallographic Object-Oriented Toolkit (COOT) and phenix.refine [22 23]. The data collection and refinement statistics are given in Supplementary Table S2. Structural images were generated by PyMol [24].

Declarations

Data availability. The atomic coordinates and structure factors for BaCcpC-IBD (PDB ID 7DMW) have benn deposited in the RCSB Protein Data Bank , www.pdb.org.

Acknowledgements

The authors acknowledge the use of beamline 7A at Pohang Accelerator Laboratory, Pohang, Republic of Koreas.

Author contributions

W. Liu and J. Chen conducted most of the experiments. W. Liu, and J. Chen prepared figures and tables. CQ and YX conceived and designed the experiments. YD, CQ, and YX performed the experiments. NCH, CQ, and YX analyzed the data and wrote the manuscript with contributions from all the other authors. CQ and YX directed and supervised the research.

Funding

This work was supported by the natural science foundation of Liaoning province (grant no. 2019-MS-065 to Y. Xu), the key lab of marine bioactive substance and modern analytical technique, SOA (grant no. MBSMAT-2019-05 to L. Jin), the Program for Liaoning Excellent Talents in University (Grant No. LJQ2015030 to Y. Xu), the Dalian High level Talents Innovation support Plan Project (Grant No. 2019CT09 to C. Quan), the Fundamental Research Funds for the Central Universities (Grant No. DC201502020203 to Y. Xu, Grant No. DC201502020201 to C. Quan), and a National Research Foundation of Korea (NRF) grant funded by the Korean government (MOE) (Grant No. NRF-2017R1D1A1B03033087 and 2017M3A9F6029736).

References

1 Krebs, H. A., Kay, J. & Weitzman, P. D. J. *Krebs' citric acid cycle : half a century and still turning*. (Biochemical Society, 1987).

2 Strasters, K. C. & Winkler, K. C. Carbohydrate Metabolism of *Staphylococcus aureus*. *J Gen Microbiol* **33**, 213-229, doi:10.1099/00221287-33-2-213 (1963).

3 Sonenshein, A. L. Control of key metabolic intersections in *Bacillus subtilis*. *Nat Rev Microbiol* **5**, 917-927, doi:10.1038/nrmicro1772 (2007).

4 Fujita, Y. Carbon catabolite control of the metabolic network in *Bacillus subtilis*. *Biosci Biotechnol Biochem* **73**, 245-259, doi:10.1271/bbb.80479 (2009).

5 Richardson, A. R., Somerville, G. A. & Sonenshein, A. L. Regulating the Intersection of Metabolism and Pathogenesis in Gram-positive Bacteria. *Microbiol Spectr* **3**, doi:10.1128/microbiolspec.MBP-0004-2014 (2015).

6 Kim, H. J., Roux, A. & Sonenshein, A. L. Direct and indirect roles of CcpA in regulation of *Bacillus subtilis* Krebs cycle genes. *Mol Microbiol* **45**, 179-190, doi:10.1046/j.1365-2958.2002.03003.x (2002).

7 Sonenshein, A. L. CodY, a global regulator of stationary phase and virulence in Gram-positive bacteria. *Curr Opin Microbiol* **8**, 203-207, doi:10.1016/j.mib.2005.01.001 (2005).

8 Hartmann, T. *et al.* Catabolite control protein E (CcpE) is a LysR-type transcriptional regulator of tricarboxylic acid cycle activity in *Staphylococcus aureus*. *J Biol Chem* **288**, 36116-36128, doi:10.1074/jbc.M113.516302 (2013).

9 Jourlin-Castelli, C., Mani, N., Nakano, M. M. & Sonenshein, A. L. CcpC, a novel regulator of the LysR family required for glucose repression of the citB gene in *Bacillus subtilis*. *J Mol Biol* **295**, 865-878, doi:10.1006/jmbi.1999.3420 (2000).

10 Maddocks, S. E. & Oyston, P. C. Structure and function of the LysR-type transcriptional regulator (LTTR) family proteins. *Microbiology* **154**, 3609-3623, doi:10.1099/mic.0.2008/022772-0 (2008).

11 Huffman, J. L. & Brennan, R. G. Prokaryotic transcription regulators: more than just the helix-turn-helix motif. *Current Opinion in Structural Biology* **12**, 98-106 (2002).

12 Aravind, L., Anantharaman, V., Balaji, S., Babu, M. M. & Iyer, L. M. The many faces of the helix-turn-helix domain: transcription regulation and beyond. *FEMS Microbiol Rev* **29**, 231-262, doi:10.1016/j.femsre.2004.12.008 (2005).

13 Pérez-Rueda, E. & Collado-Vides, J. Common History at the Origin of the Position–Function Correlation in Transcriptional Regulators in Archaea and Bacteria. *Journal of Molecular Evolution* **53**, 172-179 (2001).

14 Maddocks, S. E. & Oyston, P. C. F. Structure and function of the LysR-type transcriptional regulator (LTTR) family proteins. *Microbiology (Reading)* **154**, 3609-3623, doi:10.1099/mic.0.2008/022772-0 (2008).

15 Picossi, S., Belitsky, B. R. & Sonenshein, A. L. Molecular mechanism of the regulation of *Bacillus subtilis* gltAB expression by GltC. *J Mol Biol* **365**, 1298-1313, doi:10.1016/j.jmb.2006.10.100 (2007).

16 Ding, Y. *et al.* Metabolic sensor governing bacterial virulence in *Staphylococcus aureus*. *Proc Natl Acad Sci U S A* **111**, E4981-4990, doi:10.1073/pnas.1411077111 (2014).

17 Chen, J. *et al.* Structural and Biochemical Analysis of the Citrate-Responsive Mechanism of the Regulatory Domain of Catabolite Control Protein E from *Staphylococcus aureus*. *Biochemistry* **57**, 6054-6060, doi:10.1021/acs.biochem.8b00671 (2018).

18 Kim, Y. *et al.* Crystal structure of the ligand-binding domain of a LysR-type transcriptional regulator: transcriptional activation via a rotary switch. *Mol Microbiol* **110**, 550-561, doi:10.1111/mmi.14115 (2018).

19 Tyrrell, R. *et al.* The structure of the cofactor-binding fragment of the LysR family member, CysB: a familiar fold with a surprising subunit arrangement. *Structure* **5**, 1017-1032, doi:10.1016/s0969-2126(97)00254-2 (1997).

20 Otwinowski, Z. & Minor, W. Processing of X-ray diffraction data collected in oscillation mode. *Method Enzymol* **276**, 307-326, doi:Doi 10.1016/S0076-6879(97)76066-X (1997).

21 Adams, P. D. *et al.* PHENIX: building new software for automated crystallographic structure determination. *Acta Crystallogr D* **58**, 1948-1954 (2002).

22 Emsley, P. & Cowtan, K. Coot: model-building tools for molecular graphics. *Acta crystallographica. Section D, Biological crystallography* **60**, 2126-2132, doi:10.1107/S0907444904019158 (2004).

23 Afonine, P. V. *et al.* Towards automated crystallographic structure refinement with phenix.refine. *Acta Crystallogr D Biol Crystallogr* **68**, 352-367, doi:10.1107/S0907444912001308 (2012).

24 DeLano, W. L. Use of PYMOL as a communications tool for molecular science. *Abstr Pap Am Chem S* **228**, U313-U314 (2004).

Figures

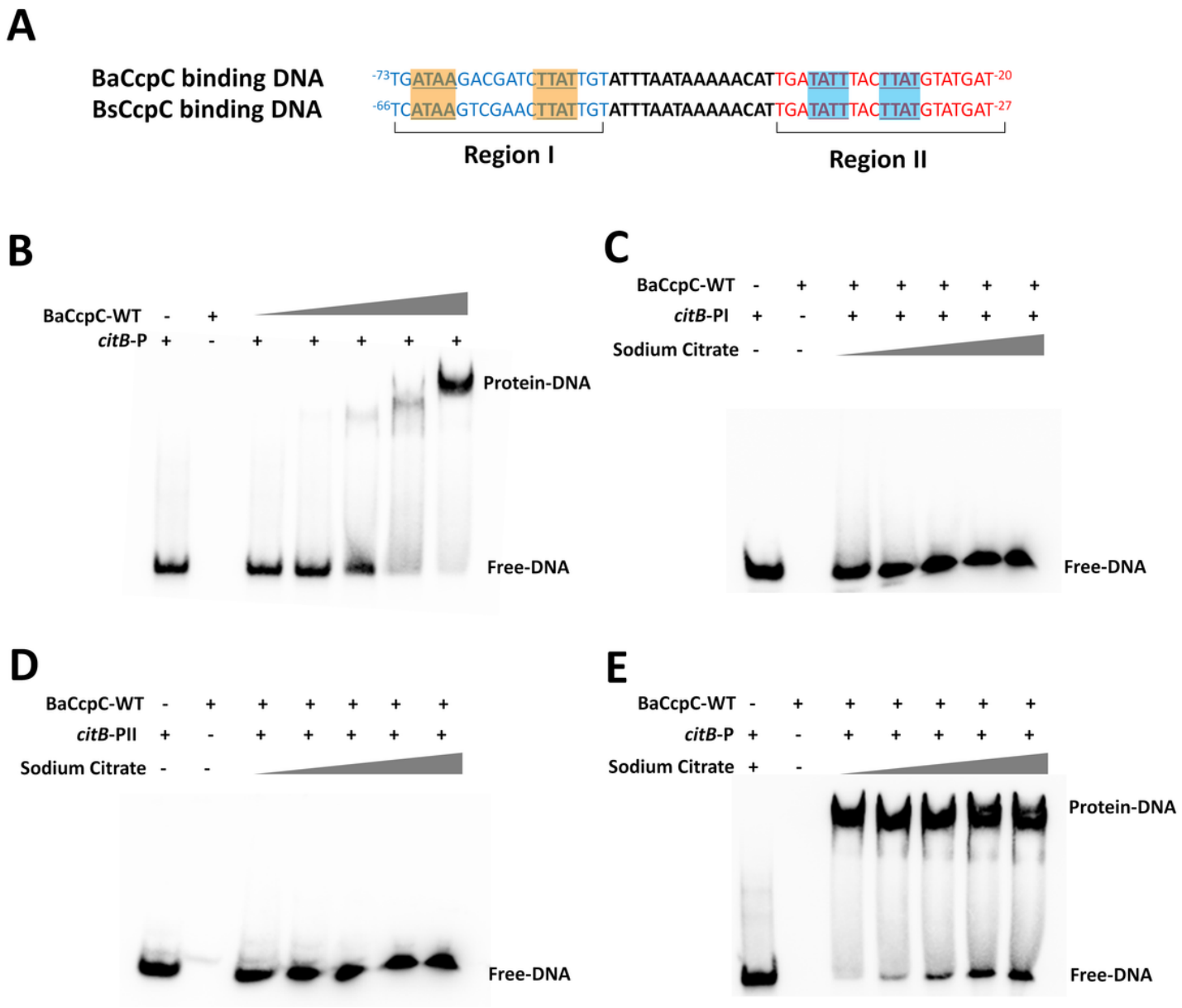

Figure 1

citB promoter-binding properties of BaCcpC. (A) Comparison of the citB promoter regions from B. amyloliquefaciens (upper) and B. subtilis (bottom). DNA-binding boxes are indicated in bold and underlined. EMSA experiment of BaCcpC with (B) The citB promoter, (C) region I in the citB promoter region, (D) region II in the citB promoter region, and (E) the citB promoter with various concentrations of sodium citrate.

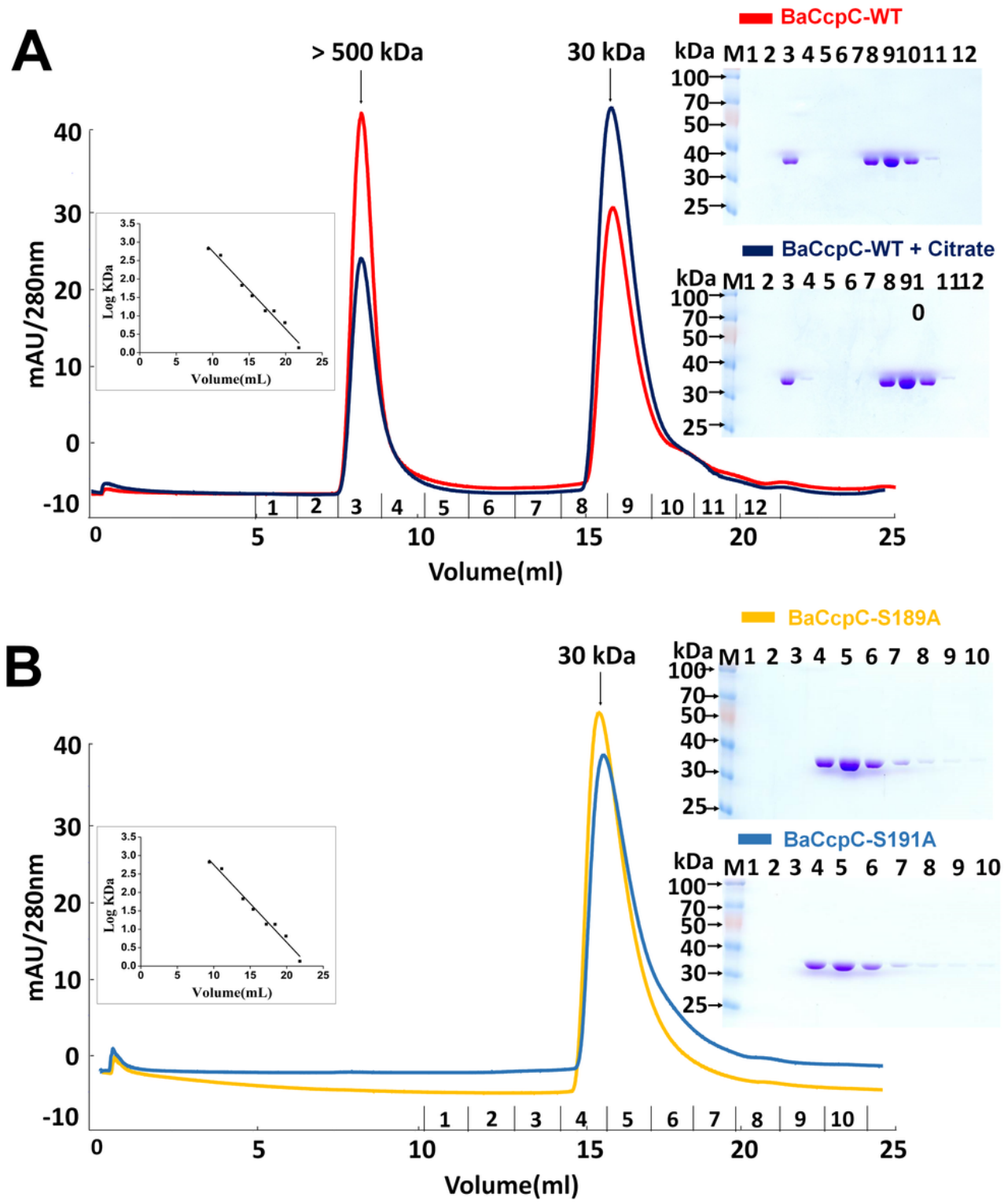

Figure 2

Oligomeric state of BaCcpC. (A) Analysis of the oligomeric state of BaCcpC in the presence or absence of citrate. (B) Analysis of the oligomeric states of BaCcpC-S189A and BaCcpC-S191A.

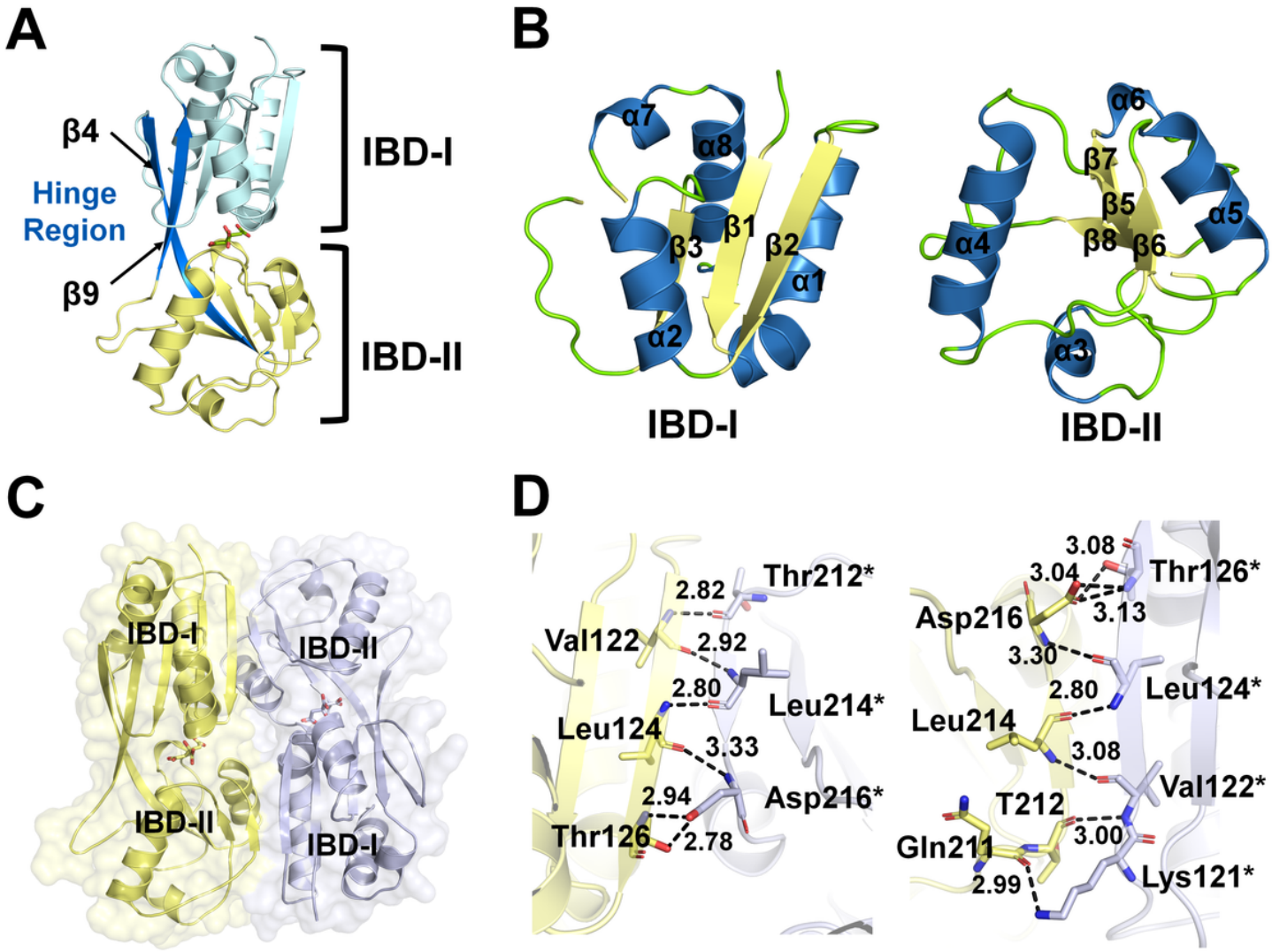

Figure 3

Overall structure of BaCcpC-IBD. (A) Monomer structure of BaCcpC-IBD. The hinge regions, consisting of β4- and β9-strands, are indicated in blue. Citrate molecules are located between the IBD-I and IBD-II subdomains. (B) Close-up view of the IBD-I and IBD-II subdomains of BaCcpC-IBD. (C) Dimer of BaCcpC-IBD. (D) Close-up view of the interactions in the dimer interface.

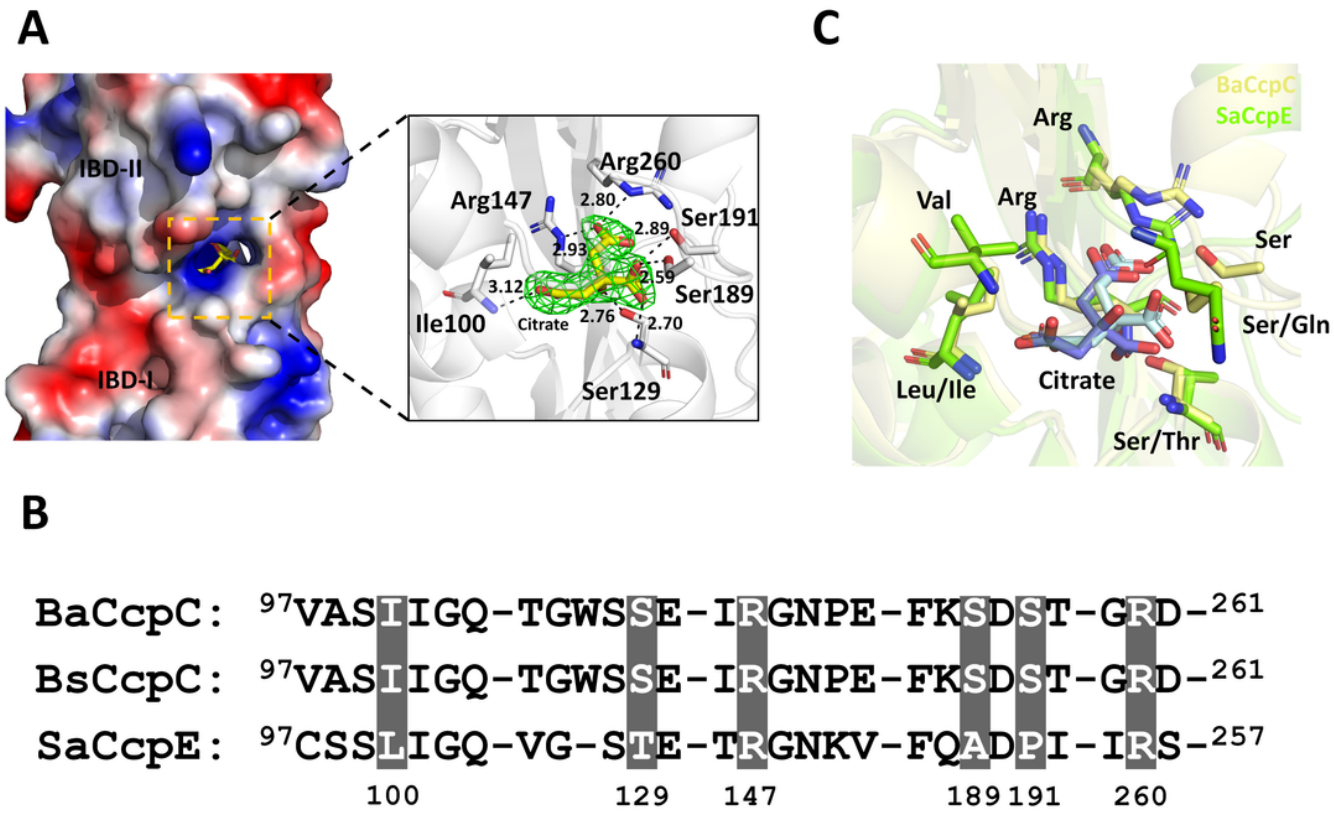

Figure 4

Citrate binding site of BaCcpC-IBD. (A) Citrate binding to the interface between IBD-I and II of BaCcpC-IBD. (Insert) Interaction between citrate and BaCcpC-IBD. 2Fo-Fc electron (green mesh, 1σ) density map for citrate molecules. (B) Partial sequence alignment of the citrate binding sites of BaCcpC, BsCcpC, and SaCcpE. (C) Superimposition of the citrate binding sites of the IBD of BaCcpC (yellow) and SaCcpC (green).

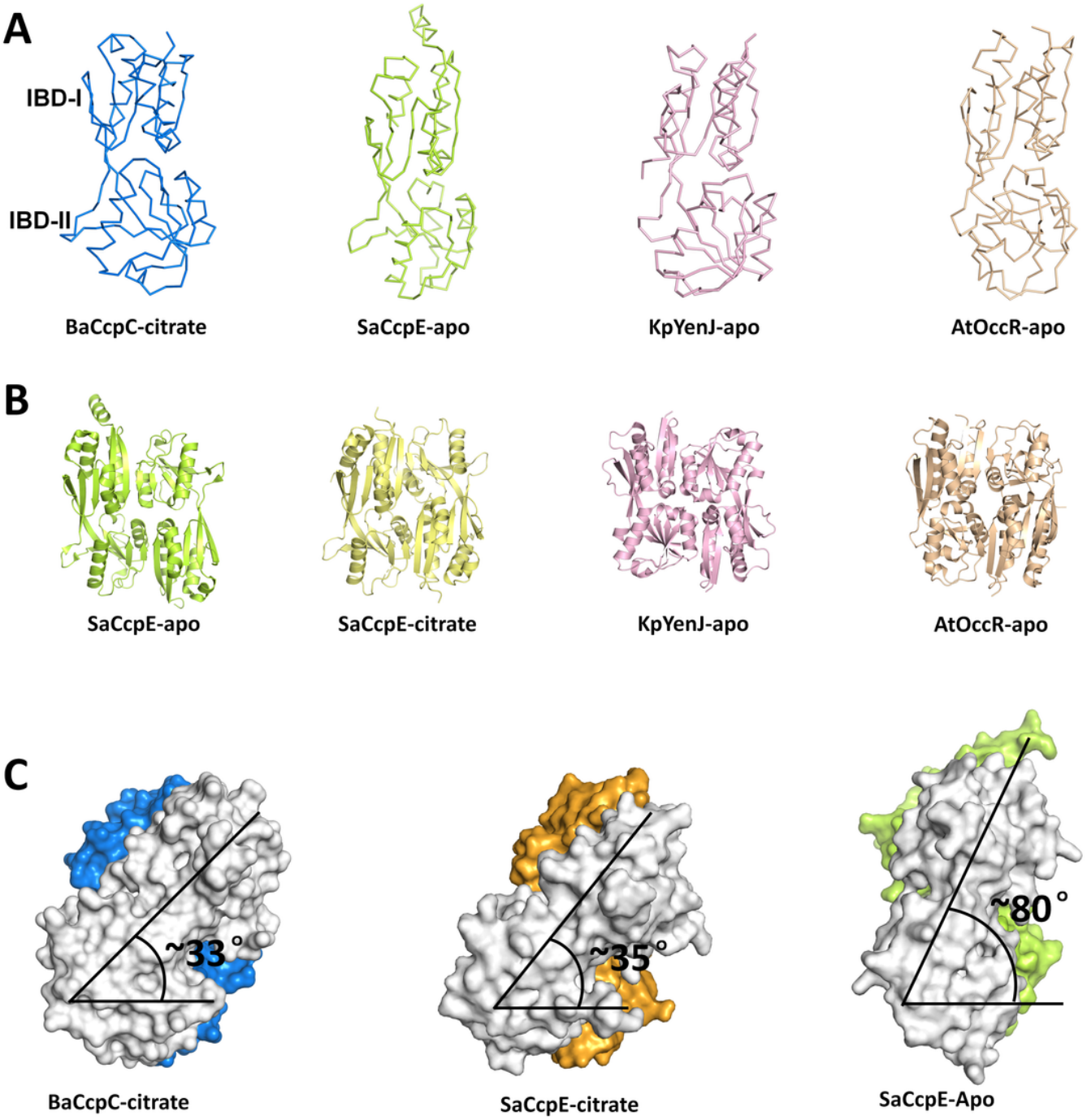

Figure 5

Structural comparison of BaCcpC-IBD with the LTTR family. (A) Ribbon representations of the IBDs (or CBDs) of BaCcpC, SaCcpE, KpYneJ and AtOccR, which consist of two subdomains. (B) Dimers of BaCcpC, SaCcpE, KpYneJ, and AtOccR, showing the tail-to-tail arrangement. (C) Comparison of rotation in BaCcpC-IBD-citrate, SaCcpE-IBD-citrate, and SaCcpE-IBD-apo dimers.

Supplementary Files

This is a list of supplementary files associated with this preprint. Click to download.

- ScientificRCcpCSpplementalInformation.docx